

(Fig. 4F) fits with their being recruited to promoters as a complex.

Given that BAP1 KO mice develop MDS, we investigated whether *BAP1* mutations occur in human MDS by full-length resequencing of *BAP1* in 32 paired tumor and normal samples from patients with de novo MDS. We identified a patient with a frameshift mutation that causes premature termination within the UCH catalytic domain of BAP1. Analysis of matched normal DNA did not identify the frameshift allele, which is consistent with somatic acquisition of the frameshift *BAP1* mutation by the MDS clone (fig. S14). The patient with the somatic *BAP1* mutation presented with refractory cytopenias and multilineage dysplasia, similar to the multilineage dysplasia and cytopenias seen in our murine model. Mutational profiling revealed that this patient was WT for known MDS mutations, including *TET2*, *ASXL1*, *EZH2*, *NRAS*, *C-KIT*, *FLT3*, *IDH1*, and *IDH2*, and had del(20)(q11.2q13.3) as the sole cytogenetic abnormality on metaphase chromosome analysis. In a separate microarray data set (25), *BAP1* mRNA expression was reduced significantly in CD34⁺ cells from MDS patients as compared to healthy controls (fig. S15), which is in keeping with *BAP1* being a tumor suppressor. To mimic *BAP1* haploinsufficiency, we characterized heterozygous *Bap1*^{fl/+} creERT2⁺ mice after tamoxifen treatment. Loss of one copy of *Bap1* caused very mild, but progressive, hema-

tological defects (fig. S16), which is important because the frameshift mutation identified in the patient is heterozygous.

Our results identify a previously unknown and potent tumor suppressor function for BAP1 in myeloid neoplasia. The BAP1 ortholog in *Drosophila*, called Calypso, suppresses *hox* gene expression (17), but we did not see increased *Hox* gene expression in BAP1 KO cells (fig. S17). Divergent epigenetic functions for fly and vertebrate BAP1 might reflect the fact that the HCF-1 binding motif conserved in vertebrate BAP1 (16, 20) is absent from Calypso. We propose that BAP1 forms a core complex with HCF-1 and OGT that can differentially recruit additional histone-modifying enzymes to regulate gene expression and thereby preserve normal hematopoiesis. It will be interesting to determine whether *Bap1* deficiency restricted to nonhematopoietic mouse tissues also promotes tumor development.

References and Notes

1. J. W. Harbour *et al.*, *Science* **330**, 1410 (2010).
2. D. E. Jensen *et al.*, *Oncogene* **16**, 1097 (1998).
3. D. E. Jensen, F. J. Rauscher 3rd, *Cancer Lett.* **143** (suppl. 1), S13 (1999).
4. G. Guo *et al.*, *Nat. Genet.* **44**, 17 (2011).
5. M. H. Abdel-Rahman *et al.*, *J. Med. Genet.* **48**, 856 (2011).
6. J. R. Testa *et al.*, *Nat. Genet.* **43**, 1022 (2011).
7. T. Wiesner *et al.*, *Nat. Genet.* **43**, 1018 (2011).
8. J. Seibler *et al.*, *Nucleic Acids Res.* **31**, e12 (2003).
9. J. W. Vardiman *et al.*, *Blood* **114**, 937 (2009).

10. S. H. Beachy, P. D. Aplan, *Hematol. Oncol. Clin. North Am.* **24**, 361 (2010).
11. S. J. Corey *et al.*, *Nat. Rev. Cancer* **7**, 118 (2007).
12. A. Klinakis *et al.*, *Nature* **473**, 230 (2011).
13. M. Krüger *et al.*, *Cell* **134**, 353 (2008).
14. N. Kobayashi *et al.*, *Gene* **396**, 236 (2007).
15. M. E. Sowa, E. J. Bennett, S. P. Gygi, J. W. Harper, *Cell* **138**, 389 (2009).
16. Y. J. Machida, Y. Machida, A. A. Vashisht, J. A. Wohlschlegel, A. Dutta, *J. Biol. Chem.* **284**, 34179 (2009).
17. J. C. Scheuermann *et al.*, *Nature* **465**, 243 (2010).
18. V. Gelli-Boyer *et al.*, *Br. J. Haematol.* **145**, 788 (2009).
19. O. Abdel-Wahab *et al.*, *Leukemia* **25**, 1200 (2011).
20. S. Misaghi *et al.*, *Mol. Cell. Biol.* **29**, 2181 (2009).
21. F. Capotosti *et al.*, *Cell* **144**, 376 (2011).
22. S. Daou *et al.*, *Proc. Natl. Acad. Sci. U.S.A.* **108**, 2747 (2011).
23. T. M. Kristie, Y. Liang, J. L. Vogel, *Biochim. Biophys. Acta* **1799**, 257 (2010).
24. A. Pellagatti *et al.*, *Br. J. Haematol.* **125**, 576 (2004).
25. T. A. Graubert *et al.*, *Nat. Genet.* **44**, 53 (2011).

Acknowledgments: We thank members of the Dixit and Martin laboratories for advice and discussions and core laboratories for technical assistance.

Supplementary Materials

www.sciencemag.org/cgi/content/full/science.1221711/DC1
Materials and Methods
Figs. S1 to S17
References

9 March 2012; accepted 25 July 2012
Published online 9 August 2012;
10.1126/science.1221711

Unicellular Cyanobacterium Symbiotic with a Single-Celled Eukaryotic Alga

Anne W. Thompson,^{1*} Rachel A. Foster,^{2*} Andreas Krupke,² Brandon J. Carter,¹ Niculina Musat,^{2†} Daniel Vaultot,³ Marcel M. M. Kuypers,² Jonathan P. Zehr^{1‡}

Symbioses between nitrogen (N)₂-fixing prokaryotes and photosynthetic eukaryotes are important for nitrogen acquisition in N-limited environments. Recently, a widely distributed planktonic uncultured nitrogen-fixing cyanobacterium (UCYN-A) was found to have unprecedented genome reduction, including the lack of oxygen-evolving photosystem II and the tricarboxylic acid cycle, which suggested partnership in a symbiosis. We showed that UCYN-A has a symbiotic association with a unicellular prymnesiophyte, closely related to calcifying taxa present in the fossil record. The partnership is mutualistic, because the prymnesiophyte receives fixed N in exchange for transferring fixed carbon to UCYN-A. This unusual partnership between a cyanobacterium and a unicellular alga is a model for symbiosis and is analogous to plastid and organismal evolution, and if calcifying, may have important implications for past and present oceanic N₂ fixation.

Nitrogen (N) is a primary nutrient whose availability constrains the productivity of the biosphere (1). Some bacteria and archaea can fix N₂ into biologically available ammonium and are important in the N cycle of terrestrial ecosystems and the global ocean. Although photosynthetic carbon (C) fixation evolved in eukaryotes through endosymbiosis of cyanobacteria that resulted in the chloroplast, no N₂-fixing plastids or N₂-fixing eukaryotes are known.

Nonetheless, N₂-fixing symbioses are common in terrestrial environments between bacteria or cyanobacteria and multicellular plants. In the oceans, there are microscopic observations of probable symbioses between N₂-fixing cyanobacteria and single-celled eukaryotic algae (2), although the nature of the interactions, if any, are unclear, except between the heterocystous N₂-fixing cyanobacteria and their associated diatoms (3).

Recently, a geographically widespread uncultivated diazotrophic cyanobacterium (UCYN-A) (4) was found to have an unusual degree of genomic streamlining suggestive of obligate symbiosis. The streamlined genome of UCYN-A (1.44 million base pairs) lacks photosystem II (PS II: the oxygen-evolving component of the photosynthetic apparatus), RuBisCo (ribulose-1,5-bisphosphate carboxylase-oxygenase that fixes CO₂), and the tricarboxylic acid cycle (TCA), features that usually define cyanobacteria (5, 6). UCYN-A requires organic carbon for energy (although it may obtain some energy through cyclic photophosphorylation around PS I) and biosynthesis, as well as a number of specific amino acids and nucleotides (5, 6). We propose the name *Candidatus* Atelocyanobacterium thalassa for UCYN-A. Dissolved organic carbon concentrations in the ocean are typically low, particularly for labile compounds such as glucose that UCYN-A would require (it has a complete gly-

¹Ocean Sciences, University of California, Santa Cruz, CA 95064, USA. ²Max-Planck-Institut für Marine Mikrobiologie, Bremen, Germany D-28359. ³UPMC (Paris-06) and CNRS, UMR 7144, Station Biologique, Plage G. Tessier 29680 Roscoff, France.

*These authors contributed equally to this work.

†Present address: Department of Isotope Biogeochemistry, UFZ-Helmholtz Centre for Environmental Research, Leipzig 04318, Germany.

‡To whom correspondence should be addressed. E-mail: zehrj@ucsc.edu

colysis pathway). Because UCYN-A has a complete suite of nitrogenase genes and related genes required for nitrogen fixation, it was hypothesized that UCYN-A provides fixed nitrogen in exchange for fixed carbon from a symbiotic partner (5, 7).

We tested different possible partner phytoplankton populations in seawater samples from the North Pacific Ocean (Fig. 1, fig. S1, and table S1) for the presence of symbiotic UCYN-A by screening flow-cytometrically sorted cells with a UCYN-A-specific quantitative PCR (qPCR) assay for the nitrogenase gene (*nifH*) (8). The UCYN-A genome had been obtained with this approach (6), but the seawater was first concentrated by vacuum filtration before sorting, which dislodged the UCYN-A from their associated cells (fig. S1). Here, we used a similar flow sorting procedure, but instead, raw seawater that had not been preserved or concentrated was immediately sorted and resulted in detection of most (63 to 94%) of the UCYN-A *nifH* genes in the sorted photosynthetic picoeukaryote population (PPE) (1- to 3- μ m-diameter cells) rather than other pigmented and nonpigmented cells (sorted populations displayed in Fig. 1). The data unequivocally showed that UCYN-A is associated with photosynthetic picoeukaryotic cells. These results explain the reports of UCYN-A *nifH* in filter-fractionated samples from the California Coast (0.8- to 3- μ m and 3- to 200- μ m fractions) (9) and Station ALOHA (1- to 3- μ m fraction) (5). We now only observe an enriched population of free UCYN-A cells (0.2 to 1 μ m) after seawater concentration by vacuum filtration, freezing for storage purposes, and resuspension in sterile seawater, which apparently disrupts the fragile association (fig. S1). UCYN-A appears to be in a loose extracellular association (epiphytic) that

is easily dislodged, which explains why there is some amplification of UCYN-A *nifH* from outside the region of the sorted photosynthetic picoeukaryote population (table S1). This delicate association is similar to microscopic observations of other probable marine plankton symbioses, including the mixed populations of unicellular *Synechococcus*- and *Crocospaera*-like unicellular cyanobacteria housed in the girdle of *Dinophysis* (dinoflagellates) (10).

The marine picoeukaryotic population defined by flow cytometry is extremely diverse (11–13). Therefore, to identify the specific cells associated with UCYN-A, we compared universal 18S ribosomal RNA (rRNA) and 16S rRNA gene clone libraries that were amplified from sorted samples of the entire picoeukaryote population to those from sorted single picoeukaryote cells (table S1). Single cells and the entire picoeukaryote population were initially screened for UCYN-A by *nifH* qPCR. As expected, the partial 18S rRNA gene sequences [\sim 730 base pairs (bp)] derived from the entire picoeukaryote population sorts were diverse and included sequences from several classes of marine picoeukaryotes (Fig. 2 and table S3). 16S rRNA gene sequences amplified from the entire picoeukaryote population sorts were also diverse and confirmed the presence of UCYN-A in these populations (table S3). However, amplification of the 18S rRNA gene (using nested PCR) from single UCYN-A *nifH*-positive sorted picoeukaryote cells yielded exclusively prymnesiophyte sequences (Fig. 2 and table S4).

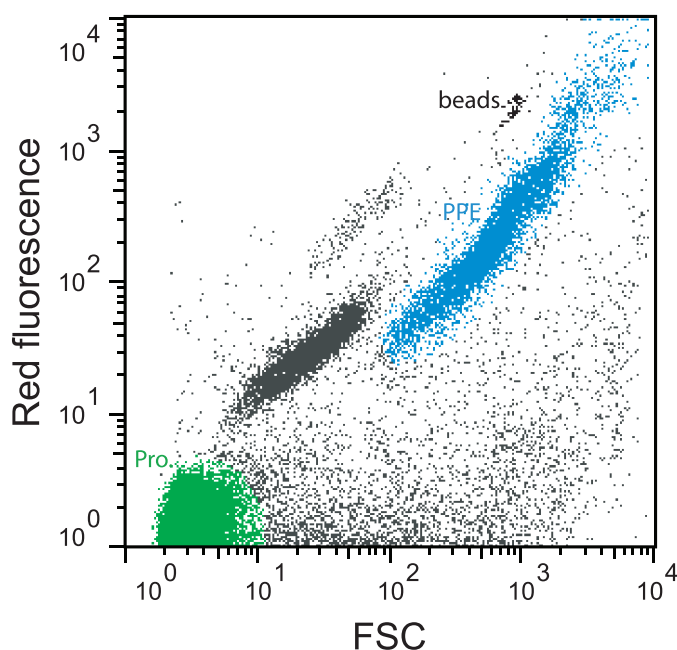
The partial 18S rRNA gene sequences [or “partner” sequences from the Ek555/1269 primer amplicon, GenBank accession nos. JX291679 to JX291804 and JX291547 to JX291678], derived from 12 single UCYN-A-*nifH*-positive picoeu-

karyotic cells, were greater than 99.5% identical to each other and had best BLASTn hits (>99% identical) to a sequence derived from sorted picoplankton from the oligotrophic South Pacific Ocean (GenBank accession no. FJ537341, BIOSOPE T60.34, sample T60, Station STB11, -107.29° E, -27.77° S) (14) (Fig. 2). A metagenome from sorted photosynthetic picoeukaryotes of the same sample (BIOSOPE, sample T60) also contained numerous DNA sequence reads (mean length of 340 bp) that were almost identical (99 to 100%) to the UCYN-A genome. Samples from an adjacent station (STB7, samples T39 and T40) contained neither good matches to the UCYN-A genome nor the partner partial 18S rRNA gene sequence we identified (table S2 and fig. S2). Assembly of the UCYN-A reads from sample T60 covered 12.4% of the UCYN-A genome (table S2), providing additional evidence that UCYN-A is associated with the picoeukaryotes and that the UCYN-A partner is the same in the oligotrophic North and South Pacific Oceans.

We examined the phylogeny of the full-length 18S rRNA gene of the BIOSOPE environmental sequence (T60.34) (UCYN-A partner sequence best BLASTn hit) relative to the diverse prymnesiophyte class (11, 15, 16). The BIOSOPE T60.34 sequence clustered with the calcareous nanoplankton *Braarudosphaera bigelowii* (17–20) and with *Chrysochromulina parkeae* (21, 22), which may contain calcified scales as well (23) (Fig. 2). *B. bigelowii* appears to represent several pseudo-cryptic species that are all easily differentiated from other calcareous phytoplankton by their distinct pentagonal plates (19). Production of calcified plates by the UCYN-A partner is an intriguing possibility, because calcareous phytoplankton are important in the vertical flux of carbon and nitrogen in the oceans. Sedimentary records from the late Cretaceous show fossils of *Braarudosphaera* species in open ocean sediments (24, 25), suggesting that the UCYN-A symbiosis could be ancient and could potentially be studied in a paleo-oceanographic context. However, prymnesiophytes (for example, *Emiliania huxleyi*) have complex life histories in which form (in particular calcification) and behavior change dramatically between haploid and diploid life stages [references in (26)]. Because the life-history stage of the partner cells in the natural populations of this study is unknown and sample processing could have dissolved or removed plates, whether or not the partner is calcifying could not be determined. Calcification of the partner cell could be an important facet in its symbiosis with UCYN-A, because it could provide a mechanism for stabilizing an extracellular association.

Prymnesiophytes are typically free-living and photosynthetic and therefore could provide organic C for an associated photoheterotroph like UCYN-A. To test this hypothesis, we applied a halogenated in situ hybridization nanometer-scale secondary ion mass spectrometry (HISH-SIMS) approach to natural phytoplankton populations

Fig. 1. Example flow cytogram of cell populations in unpreserved seawater that were targeted in this study. Red fluorescence is a measure of chlorophyll a concentration per cell. Forward scatter (FSC) is a proxy for cell size. Beads 3 μ m in diameter (black) were used for reference. Cell populations indicated are photosynthetic picoeukaryotes (PPE, blue), *Prochlorococcus* (*Pro.*, green), and cells (gray) that are not PPE or *Pro.* Coloring of each population indicates the sort gates used. Most UCYN-A *nifH* gene copies (63 to 94%) were amplified from the PPE population (table S1). Flow cytograms of all samples used in this study are presented in fig. S1.



from Station ALOHA (27) that were amended with $^{15}\text{N}_2$ and ^{13}C -bicarbonate (H^{13}CO_3) and incubated under in situ conditions. The photosynthetic picoeukaryote cells (diameter 1 to 3 μm) were subsequently sorted by flow cytometry, preserved, and processed for HISH-SIMS (27, 28). A highly specific oligonucleotide probe for the UCYN-A 16S rRNA gene (UCYN-732) (27) confirmed the presence of 278 UCYN-A cells among the sorted photosynthetic picoeukaryote population. Most (163, 59%) of the UCYN-A cells (diameter 0.31 to 0.92 μm) remained associated with a larger

partner cell (diameter 0.99 to 1.76 μm) during sample processing. UCYN-A cells were mainly observed at one end of the partner cell in what appeared to be an indentation (Fig. 3A). Numerous UCYN-A cells (107, 38%) were dislodged from their eukaryotic partners during HISH-SIMS sample processing (the cells were initially attached, otherwise they would not have been sorted by flow cytometry) and observed without an associated cell. Some (3%) of the UCYN-A cells identified by HISH were present as pairs located at opposite ends of a single partner cell (Fig. 3A). In other

planktonic symbioses involving cyanobacteria (e.g., diatom symbionts with filamentous heterocyst-forming cyanobacteria), the cyanobacteria migrate to polar ends of the larger partner cells before cell division of the host (29). Similarly, the partner cells with multiple associated UCYN-A cells may have been dividing, because the incubation period was longer than a typical cell division cycle (36 hours). Measurements of scanning electron micrographs (SEMs) of individual *B. bigelowii* cells from enrichments of coastal waters show three size classes, the smallest of which corresponds

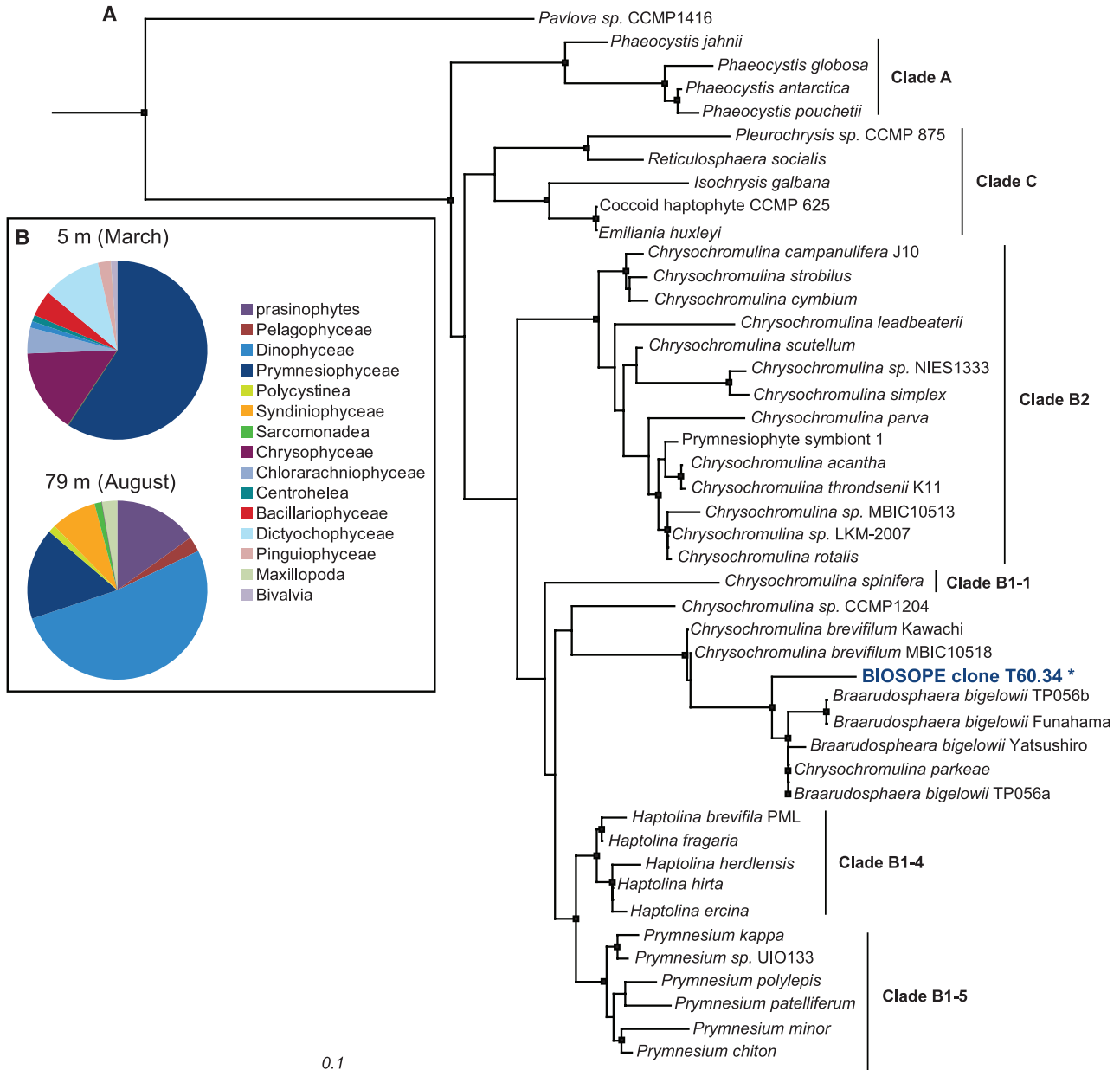


Fig. 2. Diversity and phylogeny of UCYN-A *nifH*-positive sorted picoeukaryote populations and single cells from 5-m and 79-m depths at Station ALOHA. **(A)** Maximum-likelihood tree (PhyML) of selected cultured prymnesiophyte 18S rRNA gene sequences with clade assignments and genus names per (15). “BIOSOPE T60.34” sequence (blue type and asterisk) is the best BLASTn hit of the UCYN-A partner sequence amplified

from UCYN-A *nifH*-positive single photosynthetic picoeukaryotes. Node support greater than 75% is marked by black squares. **(B)** 18S rRNA gene diversity of the entire sorted picoeukaryote population that was the source of single cell sorts from March (5-m depth, cruise KM1110) and August (79-m depth, cruise HOT234) that were positive for UCYN-A *nifH* and the BIOSOPE T60.34 sequence.

to cell diameters of about 5 μm , which is larger than the UCYN-A partner cell measured here (18, 19). If calcareous plates are present on the UCYN-A partner, loss of the plates during sample processing for HISH-SIMS may result in measurement of a smaller cell diameter than cells measured by SEM. Alternatively, the UCYN-A partner may represent an additional smaller-size class of *B. bigelowii* adapted to the oligotrophic ocean.

Ten partner cells and their associated UCYN-A cells were chosen for quantitative isotopic analysis with nanoSIMS. On average, $^{13}\text{C}/^{12}\text{C}$ enrichment was lower in the UCYN-A cells than in the partner cells (average ^{13}C atom % of 1.8139 and 2.4602, respectively; Fig. 3, B and C, and table S6). Because the UCYN-A genome does not contain carbon-fixation pathways (5, 6), but photosynthetic picoeukaryotes do, we conclude that the ^{13}C enrichment in UCYN-A was due to transfer of fixed C from the eukaryotic partner. Both partner and UCYN-A were strongly ^{15}N -enriched (Fig. 3, C and D, and table S6). As only some bacteria and some archaea can fix N_2 , our nanoSIMS data provide direct evidence for active N_2 fixation by the uncultivated UCYN-A. The average $^{15}\text{N}/^{14}\text{N}$ enrichment was higher in the partner cells than in the UCYN-A cells (average ^{15}N atom % of 1.5308 and 1.2081, respectively), showing that extensive amounts (we estimate up

to 95%) of fixed N were transferred from UCYN-A to the partner cell. In contrast, little of the C (1 to 17%) fixed by the partner cell was transferred to the UCYN-A, consistent with the lower C requirements of a small slow-growing heterotrophic symbiont. The large fraction of N transferred to the partner is consistent with results from known symbioses, such as between heterocystous cyanobacteria and marine planktonic diatoms (3).

The symbiosis reported here is unusual in that it is a partnership between a prymnesiophyte and a unicellular cyanobacterium. The results provide an explanation for how the metabolically streamlined UCYN-A survives in the oligotrophic ocean, despite the lack of the TCA cycle, PS II, and some biosynthetic pathways. Tracer experiments using ^{15}N and ^{13}C clearly show that the cyanobacterium provides fixed N to the eukaryotic partner and conversely that C fixation by the eukaryotic partner can provide C to UCYN-A. Thus, the association appears to be at least a mutualistic and facultative, if not an obligate, association. It is still not known whether the cyanobacterium is an endosymbiont or lives on the surface of the prymnesiophyte. However, the sensitivity to disruption and the HISH-SIMS imaging indicates that it is a loose cell-surface association. Many of the dislodged cells observed after HISH-SIMS were located near a picoeukaryotic cell.

Because *B. bigelowii*, the closest known relative of the sequence amplified from our single-cell sorts, has calcareous plates that are easily dislodged, it is conceivable that UCYN-A is somehow associated with these plates. Sample handling and processing, in particular the HISH assay, could have dislodged or dissolved the calcium carbonate plates, releasing UCYN-A.

The association of UCYN-A with prymnesiophytes suggests that N fixed by UCYN-A may enter the microbial loop through this group of relatively abundant and globally relevant primary producers and mixotrophs (11, 16, 30, 31) and has other important implications. The UCYN-A partner may be calcifying, which has implications for the contributions of N_2 -based new production to vertical carbon fluxes (32), the sensitivity of the UCYN-A partner to ocean acidification (33), and paleo-oceanographic microfossils in sediments. Equally interesting is the existence of a planktonic unicellular N_2 -fixing symbiosis and its implications for evolution and adaptation. The presence of these simple interactions between single-celled organisms are reminiscent of those earlier primary endosymbiotic events and underscores the enigmatic absence of N_2 -fixing plastids in evolution as N_2 fixation is an energetically expensive oxygen-sensitive reaction, and nitrogenase is an ancient enzyme. Thus, the UCYN-A association is a symbiosis with a prymnesiophyte and provides an intriguing model for the evolution of N_2 fixation, and the mutualistic interactions between planktonic microorganisms.

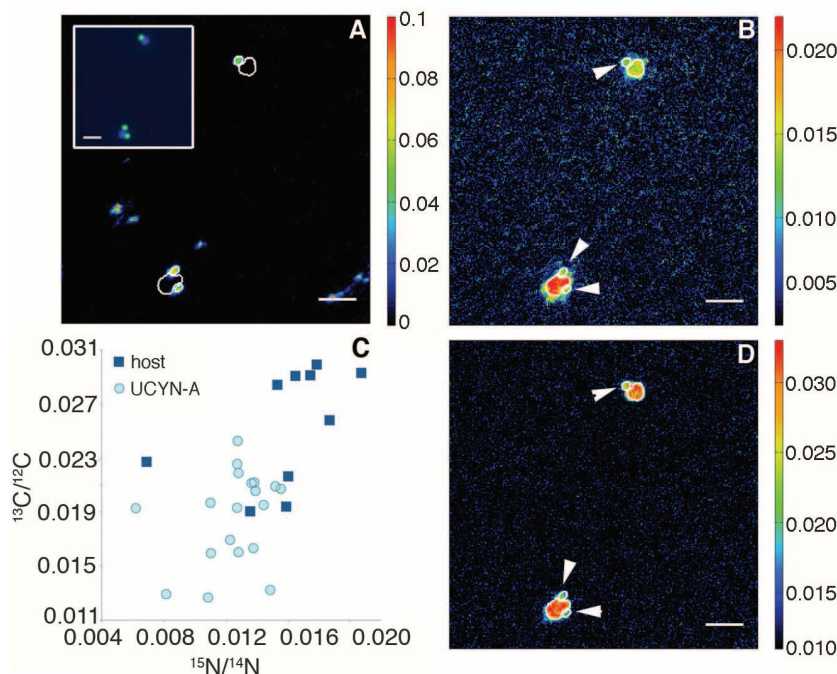


Fig. 3. Microscopy and elemental composition of two UCYN-A partner cells and their associated UCYN-A cells detected in samples from sorted picoeukaryotes analyzed by HISH-SIMS. (A) $^{19}\text{F}/^{12}\text{C}$ (HISH) labeling of UCYN-A. Inset displays labeling of the same UCYN-A cells by catalyzed reporter deposition-fluorescence in situ hybridization (green) and DAPI (4',6'-diamidino-2-phenylindole) staining of partner cell nucleus (blue). (B) The $^{13}\text{C}/^{12}\text{C}$ ratio image of UCYN-A and partner cell. (C) The $^{13}\text{C}/^{12}\text{C}$ and $^{15}\text{N}/^{14}\text{N}$ in 10 selected partner cells and their associated UCYN-A cells (table S6). (D) The $^{15}\text{N}/^{14}\text{N}$ image ratio of UCYN-A and partner cell. The white lines define regions of interest that were used for calculating $^{13}\text{C}/^{12}\text{C}$ and $^{15}\text{N}/^{14}\text{N}$ ratios. UCYN-A cells are indicated by white arrows in (B) and (D). Scale bar, 3 μm .

References and Notes

- N. Gruber, J. N. Galloway, *Nature* **451**, 293 (2008).
- E. J. Carpenter, R. A. Foster, in *Cyanobacteria in Symbiosis*, A. N. Rai, B. Bergman, U. Rasmussen, Eds. (Springer, Dordrecht, Netherlands, 2003), pp. 11–17.
- R. A. Foster *et al.*, *ISME J.* **5**, 1484 (2011).
- P. H. Moisander *et al.*, *Science* **327**, 1512 (2010).
- H. J. Tripp *et al.*, *Nature* **464**, 90 (2010).
- J. P. Zehr *et al.*, *Science* **322**, 1110 (2008).
- H. Bothe, H. J. Tripp, J. P. Zehr, *Arch. Microbiol.* **192**, 783 (2010).
- M. J. Church, C. M. Short, B. D. Jenkins, D. M. Karl, J. P. Zehr, *Appl. Environ. Microbiol.* **71**, 5362 (2005).
- L. Z. Allen *et al.*, *ISME J.* **6**, 1403 (2012).
- R. A. Foster, B. Bergman, E. J. Carpenter, *J. Phycol.* **42**, 453 (2006).
- L. Jardillier, M. V. Zubkov, J. Pearman, D. J. Scanlan, *ISME J.* **4**, 1180 (2010).
- S. Y. Moon-van der Staay, R. De Wachter, D. Vaulot, *Nature* **409**, 607 (2001).
- D. Vaulot, W. Eikrem, M. Viprey, H. Moreau, *FEMS Microbiol. Rev.* **32**, 795 (2008).
- X. L. Shi, D. Marie, L. Jardillier, D. J. Scanlan, D. Vaulot, *PLoS ONE* **4**, e7657 (2009).
- B. Edvardsen *et al.*, *Eur. J. Phycol.* **46**, 202 (2011).
- M. L. Cuvelier *et al.*, *Proc. Natl. Acad. Sci. U.S.A.* **107**, 14679 (2010).
- H. H. Gran, T. Braarud, *J. Biol. Board Can.* **1**, 279 (1935).
- K. Hagino, Y. Takano, T. Horiguchi, *Mar. Micropaleontol.* **72**, 210 (2009).
- Y. Takano, K. Hagino, Y. Tanaka, T. Horiguchi, H. Okada, *Mar. Micropaleontol.* **60**, 145 (2006).
- G. Deflandre, *C. R. Hebd. Seances Acad. Sci.* **225**, 439 (1947).
- J. C. Green, B. S. C. Leadbeater, *J. Mar. Biol. Assoc. U. K.* **52**, 469 (1972).

22. L. K. Medlin, A. G. Sáez, J. R. Young, *Mar. Micropaleontol.* **67**, 69 (2008).
23. A. Sáez *et al.*, in *Coccolithophores: From Molecular Processes to Global Impact*, H. R. Y. Thierstein, J. R. Young, Eds. (Springer, Berlin, 2004), pp. 251–269.
24. P. R. Bown, J. A. Lees, J. R. Young, Eds., *Calcareous Nannoplankton Evolution and Diversity Through Time* (Springer, Berlin and Heidelberg, 2004), pp. 481–508.
25. W. G. Siesser, T. J. Bralower, E. H. Carlo, *Proc. Ocean Drill. Prog. Sci. Results* **122**, 653 (1992).
26. E. Paasche, *Phycologia* **40**, 503 (2001).
27. Materials and methods are available as supplementary materials on Science Online.
28. N. Musat *et al.*, *Proc. Natl. Acad. Sci. U.S.A.* **105**, 17861 (2008).
29. F. J. R. Taylor, *Ann. Inst. Oceanogr.* **58**, 61 (1982).
30. M. V. Zubkov, G. A. Tarran, *Nature* **455**, 224 (2008).
31. F. Unrein, R. Massana, L. Alonso-Sáez, J. M. Gasol, *Limnol. Oceanogr.* **52**, 456 (2007).
32. D. M. Karl, M. J. Church, J. E. Dore, R. M. Letelier, C. Mahaffey, *Proc. Natl. Acad. Sci. U.S.A.* **109**, 1842 (2012).
33. S. C. Doney, V. J. Fabry, R. A. Feely, J. A. Kleypas, *Annu. Rev. Mar. Sci.* **1**, 169 (2009).

Acknowledgments: D. Bottjer and M. Hogan provided advice for $^{15}\text{N}_2$ additions. Water samples were collected with the help of S. Curless, M. Church, S. Wilson, S. Tozzi, and the captain and crew of the research vessel *Kilo Moana*. On-board flow cytometry was made possible by K. Doggett and D. Karl. Funding was provided by the Gordon and Betty Moore Foundation (J.P.Z.) and the NSF Center for Microbial Oceanography: Research and Education (C-MORE). The Max Planck Society sponsored the HISH-SIMS analysis. We thank G. Lavik (Max Planck Institute, Bremen) for advice and suggestions for data analysis.

J. Waterbury provided the scientific name for UCYN-A. D.V. was supported by PHYTOMETAGENE (JST-CNRS), METAPICO (Genoscope), and Micro B3 (funded by the European Union, contract 287589). BIOSOPE metagenome sequencing was performed at Genoscope (French National Sequencing Center) by J. Poulain. We thank H. Claustre, A. Sciandra, D. Marie, and all other BIOSOPE cruise participants. GenBank accession nos.: JX291679 to JX291804 and JX291547 to JX291678 (see table S4 for details).

Supplementary Materials

www.sciencemag.org/cgi/content/full/337/6101/1546/DC1
Materials and Methods
Figs. S1 and S2
Tables S1 to S6
References (34–46)

2 April 2012; accepted 20 July 2012
10.1126/science.1222700

Disruption of Reconsolidation Erases a Fear Memory Trace in the Human Amygdala

Thomas Agren,¹ Jonas Engman,¹ Andreas Frick,¹ Johannes Björkstrand,¹ Elna-Marie Larsson,² Tomas Furmark,¹ Mats Fredrikson¹

Memories become labile when recalled. In humans and rodents alike, reactivated fear memories can be attenuated by disrupting reconsolidation with extinction training. Using functional brain imaging, we found that, after a conditioned fear memory was formed, reactivation and reconsolidation left a memory trace in the basolateral amygdala that predicted subsequent fear expression and was tightly coupled to activity in the fear circuit of the brain. In contrast, reactivation followed by disrupted reconsolidation suppressed fear, abolished the memory trace, and attenuated fear-circuit connectivity. Thus, as previously demonstrated in rodents, fear memory suppression resulting from behavioral disruption of reconsolidation is amygdala-dependent also in humans, which supports an evolutionarily conserved memory-update mechanism.

Anxiety disorders are common, and they cause great suffering and high societal costs (1). The etiology involves amygdala-dependent memory mechanisms that link stressful events to previously neutral stimuli (2), and the amygdala has been demonstrated to be hyperresponsive across the anxiety disorders (3). Pharmacological and behavioral treatments of anxiety reduce symptomatology and amygdala activity (4) but have limited success because relapses occur (5). However, fear memories may be erased by recalling them and preventing their reconsolidation (6, 7). In rodents, the amygdala seems vital for fear memory reconsolidation (7, 8), but this has not been investigated in humans.

Fear conditioning, in which a previously neutral stimulus turns into a conditioned stimulus

(CS) through pairings with an aversive stimulus, forms a memory trace in the amygdala (2). Memory activation produces behavioral (2, 9) and autonomic fear reactions, such as skin conductance responses (SCRs) (10–12), frequently used to measure fear learning. Studies in animals (13) and anxiety patients (14) demonstrate that extinction weakens, but does not erase, fear memories. In rodents (13) and humans (15) alike, extinction attenuates conditioned fear expression through prefrontal inhibition. Fear can return after stress, be renewed when altering the environmental context, or reoccur with the passage of time (16).

By activating memories and disrupting their reconsolidation, through protein synthesis blockade local in the amygdala (8) or through systemic administration of β -adrenergic receptor antagonists (17, 18), fear memories are inhibited. Fear memory reconsolidation can also be disrupted behaviorally (6, 7, 19). In rodents, extinction of fear conditioning performed 10 or 60 min after presenting a reminder of the conditioned fear, but not after 6 or 24 hours, inhibited fear expression (7). Fear did not return in a new context, after

shock exposure, or with time. Thus, extinction conducted within, but not outside, the reconsolidation window resulted in permanent attenuation of the fear memory (7).

In humans, extinction performed within the reconsolidation interval also inhibited fear, whereas extinction training performed outside of the reconsolidation interval spared the memory and fear returned (6). In animals, the neural functions enabling fear memory formation and reconsolidation are located in the amygdala (2, 7–9, 20). In humans, lesion (21) and brain imaging studies (10–12, 22) confirm that the amygdala is a key area for fear memory encoding. To test the hypothesis that reconsolidation in humans is amygdala-mediated and that disruption of reconsolidation inactivates a memory trace in the basolateral amygdala, we performed a study combining brain imaging with a physiological measure of fear.

On day 1, twenty-two subjects (11 women) aged 24.0 ± 0.48 (mean \pm SEM) underwent fear conditioning to establish an associative fear memory (Fig. 1A and fig. S1). On day 2, the fear memory was reactivated by presenting the cue previously paired with the shock (CS+) for 2 min. Subjects were randomized into two groups. One group received extinction, consisting of repeated CS presentations with the shock withheld, 10 min after reactivation and thus within the reconsolidation interval. The other group received extinction 6 hours after the reactivation—i.e., outside of the interval. Fear expression was measured using SCRs (6, 19). On day 3, a renewal session was performed in a new environment, a magnetic resonance scanner, where shock electrodes were attached, although no shocks were delivered. SCRs were not measured for technical reasons. On day 5, subjects were exposed to unsigned shocks and then re-exposed to CS+. Return of fear was defined as the increase in SCR from the last extinction trial on day 2 to the first reinstatement trial on day 5 (Fig. 1B) (6).

First, we evaluated if the predicted behavioral reinstatement effect was present on day 5. Confirming this, increased fear responding was observed in the 6 hours, but not the 10 min group

¹Department of Psychology, Uppsala University, SE-751 42 Uppsala, Sweden. ²Department of Radiology, Oncology and Radiation Science, Uppsala University, SE-751 42 Uppsala, Sweden.

*To whom correspondence should be addressed. E-mail: thomas.agren@psyk.uu.se